JOURNAL OF AIRCRAFT
Vol. 39, No. 3, May–June 2002

Effect of Airfoil Characteristics on Aircraft Performance

Ashok Gopalarathnam* and Christopher W. McAvoy†
North Carolina State University, Raleigh, North Carolina 27695

Even with all of the advances in airfoil and aircraft design, there remains little guidance on how to tailor an airfoil to suit a particular aircraft. A two-pronged approach is presented to tailor an airfoil for an aircraft: 1) an approach in which aircraft performance simulations are used to study the effects of airfoil changes and to guide the airfoil design and 2) an analytical approach to determine expressions that provide guidance in sizing and locating the airfoil low-drag range. The analytical study shows that there is an ideal value for the lift coefficient for the lower corner of the airfoil low-drag range when the airfoil is tailored for aircraft level-flight maximum speed. Likewise, there is an ideal value for the lift coefficient for the upper corner of the low-drag range when the airfoil is tailored for maximizing the aircraft range. These ideal locations are functions of the amount of laminar flow on the upper and lower surfaces of the airfoil and also depend on the geometry, drag, and power characteristics of the aircraft. Comparison of the results from the two approaches for a hypothetical general aviation aircraft are presented to validate the expressions derived in the analytical approach.

Nomenclature

AR	=	wing aspect ratio
b	=	wing span
C_D	=	aircraft or wing drag coefficient based on S_w
C_d	=	airfoil drag coefficient based on chord
C_L	=	aircraft or wing lift coefficient based on S_w
C_l	=	airfoil lift coefficient based on chord
C_M	=	aircraft pitching moment coefficient about the center of gravity
C_m	=	airfoil pitching moment coefficient about the quarter-chord location
e	=	Oswald's efficiency factor
l_t	=	longitudinal distance from wing aerodynamic center (a.c.) to tail a.c.
M	=	Mach number
P_{av}	=	power available
P_{req}	=	power required
R	=	aircraft range
R/C	=	aircraft rate of climb
Re	=	Reynolds number
S	=	area
V_h	=	horizontal tail volume ratio
V	=	aircraft velocity
W	=	aircraft weight
W_e	=	aircraft weight without fuel
W_f	=	aircraft weight with fuel
α	=	angle of attack
β	=	$\mathrm{d}C_l/\mathrm{d}C_d$ for the low-drag line
η_p	=	propeller efficiency
ρ	=	density

Subscripts

c.g.	=	aircraft center of gravity
f	=	fuselage and other components of aircraft except wing
i	=	induced
max	=	maximum
min	=	minimum
p	=	profile
t	=	horizontal tail
w	=	wing

Superscripts

low	=	lower corner of the airfoil low-drag range
up	=	upper corner of the airfoil low-drag range
0	=	C_d intercept of the low-drag line

Introduction

WITH advances in rapid, interactive inverse design methods for airfoils[1–4] and robust analysis techniques,[1,3,5] it is now possible to custom design a family of airfoils to suit a particular application. Two recent studies[6,7] have demonstrated the suitability of an inverse approach for designing airfoils with systematic variations in the airfoil performance characteristics. Although an aircraft designer greatly benefits by having such a family of airfoils tailored for the aircraft being designed, there is also a need for an approach to select the most suitable airfoil(s) from among the candidates available. Also of benefit would be an approach that can guide further airfoil refinement efforts to better suit the aircraft application. Even with all of the advances in airfoil and aircraft design, however, there remains surprisingly little guidance in the literature on how to tailor an airfoil to suit a particular aircraft.

For example, it is well-known that airfoils with larger extents of laminar flow and lower camber tend to be more suitable for high-speed performance. It is not known, however, as to whether or not there exists an optimum combination of these airfoil characteristics. Currently, only a few references seem to exist that attempt to integrate airfoil and aircraft design. Maughmer and Somers[8] describe the development of a figure of merit for airfoil/aircraft design integration to aid in the preliminary design efforts of an aircraft. The work by Kroo,[9] although primarily devoted to the effects of trim drag and tail sizing, incorporates the effect of wing airfoil drag in the aircraft performance predictions.

In the current paper, two approaches are presented and compared for tailoring an airfoil to suit a given aircraft. The first approach involves designing a family of airfoils using the method described in Ref. 6, although airfoils from any other method or catalog could also be used. The predicted lift, drag, and pitching moment characteristics for these airfoils are then used as inputs to a multiple lifting-surface vortex lattice code to compute the viscous and induced drag of a trimmed wing–tail configuration. These drag predictions, along

Received 17 November 2001; revision received 4 March 2002; accepted for publication 7 March 2002.

*Assistant Professor, Department of Mechanical and Aerospace Engineering, Box 7910; ashok_g@ncsu.edu. Member AIAA.

†Graduate Research Assistant, Department of Mechanical and Aerospace Engineering, Box 7910; cwmcavoy@eos.ncsu.edu. Student Member AIAA.

with the engine power characteristics and estimates of the drag for the fuselage and other components, are then used in an aircraft performance prediction code. The outputs include the level-flight maximum speed and variations of performance parameters such as climb rate and range with flight speed for the aircraft. Thus, the effect of airfoil characteristics on the different performance parameters of a particular airplane are obtained. This approach has the advantages that changes in the drag due to trim effects[9–13] associated with the changes in the wing airfoil pitching moment are taken into consideration. To tailor an airfoil for a particular aircraft using this method, however, could require a considerable amount of trial and error.

The second approach involves derivation of analytical expressions for the ideal locations of the lower and upper corners of the low-drag range (drag bucket) of an airfoil to suit a particular aircraft. In this approach, the low-drag ranges of a family of airfoils with a prescribed amount of laminar flow have been described by an equation for a straight line in the airfoil C_d–C_l polar plot. The ideal C_l values for the upper and lower corners of the low-drag range are then determined by computing the variation of different aircraft performance parameters along this straight line.

The following section presents the relevant information on a hypothetical general-aviation aircraft that has been used in the subsequent sections of the paper. The next section describes the aircraft performance-simulation approach and its use in guiding the airfoil design for the wing. A section on the development of the analytical approach to size the airfoil low-drag range of the polar is then presented. Finally, the results of the analytical approach are validated by comparison with the results obtained from the performance-simulation approach with and without trim effects.

Aircraft Specifications

This section presents the relevant details of a hypothetical general-aviation aircraft used in the rest of the paper. The aircraft considered is a conventional, aft-tail configuration with a constant-speed propeller driven by a piston engine. Figure 1 shows the planview of the wing and tail geometry.

Table 1 presents the relevant specifications for the aircraft. As shown, an equivalent parasite drag area ($C_{Df}S_f$) has been assumed for the fuselage and all of the components of the airplane except the wing. The propeller efficiency has been assumed to be a constant. Although this assumption may not be true for the entire speed range of the airplane even with a constant-speed propeller, the assumption makes the available power independent of the speed and is, therefore, useful for identifying the effects of airfoil changes. Note, however, that both of the approaches discussed can readily accommodate a nonconstant propeller efficiency. The static margin (SM) has been assumed to be 10% of the wing mean aerodynamic chord (mac) for the flight speeds where the wing airfoil operates in the low-drag region of the polar.

Aircraft Performance-Simulation Approach to Study Effect of Airfoil Changes

This section describes the approach of using aircraft performance simulations to study the effect of changes to the airfoil

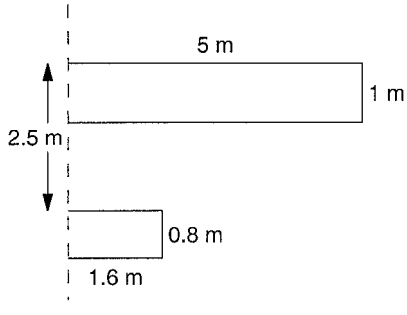

Fig. 1 Planview showing the right-side geometry of the wing and tail for the hypothetical aircraft used.

Table 1 Assumed geometry, drag, and power characteristics for the hypothetical general aviation airplane

Parameter	Value
Gross weight W	7116.8 N (1600 lbf)
Wing area, reference area S_w	10 m^2 (107.6 ft^2)
Wing aspect ratio AR	10
Equivalent parasite drag area of airplane minus wing $C_{Df}S_f$	0.18 m^2 (2.24 ft^2)
Rated engine power P_{av}	74.63 kW (100 hp)
SFC	10.7 N/s/W (0.5 lbf/h/hp)
Propeller efficiency η_p	85%, constant
Fuel volume	85.1 liters (22.5 U.S. gal)
Tail area S_t	2.56 m^2 (27.56 ft^2)
Wing-to-tail moment arm $\overline{l_t}$	2.45 m (8.04 ft)
Tail volume ratio $\overline{V_h}$	0.63
SM	10% mac
Aircraft c.g. location	44% mac

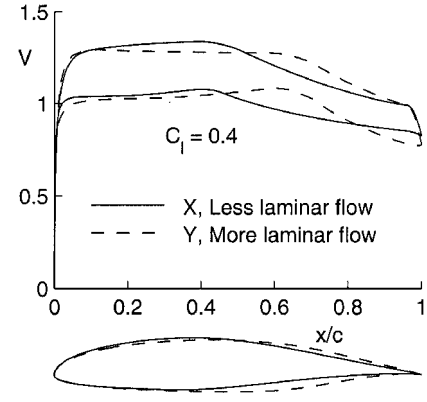

Fig. 2 Inviscid velocity distributions for airfoils X and Y.

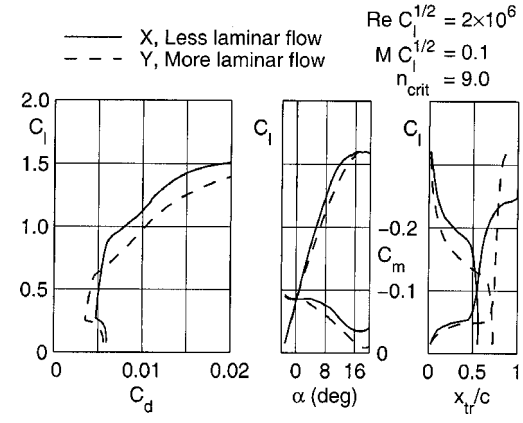

Fig. 3 Performance of airfoils X and Y predicted using XFOIL.[3]

characteristics. To describe the approach, two example airfoils have been designed using the methodology described in Ref. 6 to have the same C_l for the lower corner of the low-drag range, but with different amounts of laminar flow. In this section, the performance of the aircraft for these two airfoil choices are compared and discussed in detail. The geometries and inviscid velocity distributions for the two airfoils are shown in Fig. 2. Airfoil X has laminar flow extending to 40% chord on the upper and lower surfaces, and airfoil Y has laminar flow to 60% chord. The predicted performance for these two airfoils, obtained using XFOIL,[3] are shown in Fig. 3 for $Re\sqrt{C_l} = 2 \times 10^6$ and $M\sqrt{C_l} = 0.1$. The use of constant values for $Re\sqrt{C_l}$ and $M\sqrt{C_l}$ for the analysis of this and all of the other airfoils in this study ensures that the changes in Reynolds number Re and Mach number M with C_l due to change in the flight velocity are automatically taken into consideration. These relationships for the reduced Reynolds number Re and Mach number M can be

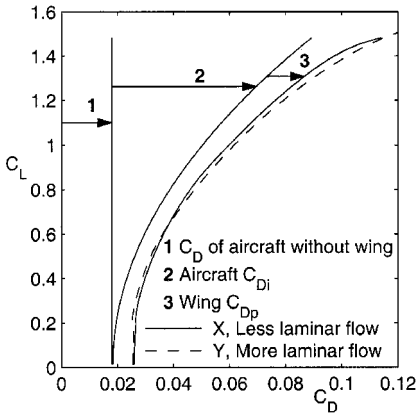

Fig. 4 Drag polar for the entire aircraft when using airfoils X and Y.

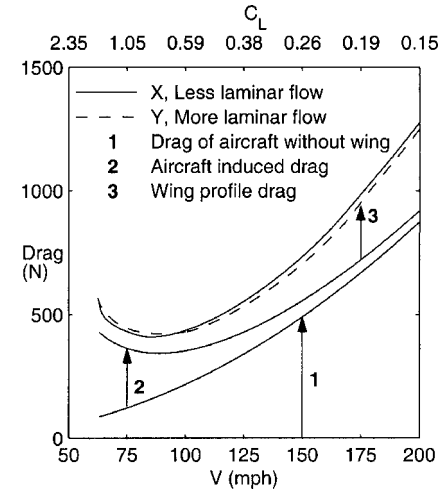

Fig. 5 Drag variation for the entire aircraft when using airfoils X and Y.

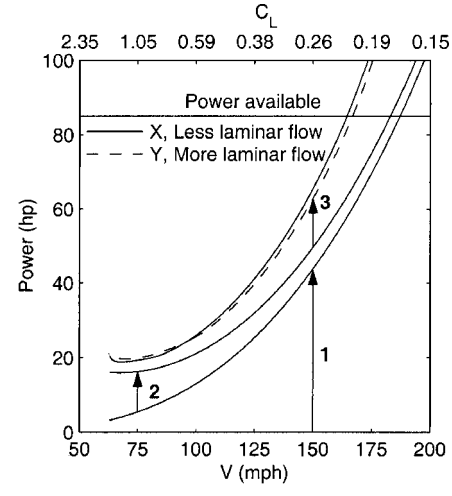

Fig. 6 Variation of the power required for level flight for the entire aircraft with the two airfoils, with contributions from the zero-lift drag of the aircraft minus wing (1), the induced drag (2), and the profile drag of the wing (3).

derived from $L \approx W$ considerations for an airplane in steady rectilinear flight.

When the drag polars for the two airfoils are compared, it is seen that, whereas airfoil Y has a lower $C_{d\,\min}$ than airfoil X resulting from greater extents of laminar flow, it also has a smaller C_l range over which the low drag is achieved, that is smaller drag bucket. More specifically, although airfoil Y has lower drag below a C_l of 0.65, above this C_l this airfoil has significantly greater C_d than airfoil X. When this result is examined, it is clear that, whereas airfoil Y will result in a higher cruise performance than X, it can also suffer from reduced climb performance. It is not clear, however, whether the benefit from the better cruise performance is worth the loss in climb performance.

As a first step in understanding the effect on aircraft performance, it is useful to consider the total aircraft drag polars (aircraft C_D vs C_L) shown in Fig. 4 for the two airfoils. The contribution from the C_D for the aircraft minus the wing (labeled 1) is considered to be independent of the choice of the wing airfoil. Furthermore, because the two airfoils X and Y have nearly the same C_m, the trimmed aircraft C_{Di} (labeled 2) is also considered to be independent of the airfoil choice. Figure 4 shows the well-known dominance of C_{Di} at highlift coefficients and, in doing so, puts in proper perspective the higher C_d of airfoil Y at these high values of C_L. The difference in C_D due to change in the airfoil section at a C_L of 1.0 is now approximately 4%, instead of the 20% difference in C_d when only the section drag polars (shown in Fig. 3) are considered.

The aircraft C_{Di} variation was obtained from a trim analysis of the wing–tail combination shown in Fig. 1. This analysis was performed using Wings, a vortex-lattice code that can handle multiple lifting surfaces. The code uses a single chordwise row of lattices and has the capability to read in the XFOIL α–C_l–C_d–C_m polar output files for the airfoils used for the lifting surfaces. Thus, the analysis method can use the airfoil drag polars and pitching moment curves for several sections along the wing span in computing the drag of the wing–tail configuration. In the current analysis, the horizontal tail incidence is adjusted to trim the aircraft, so that $C_{M\,\text{c.g.}} = 0$. In other words, for each point on the C_{Di} curve in Fig. 4, the drag contributions associated with the trim considerations have been included.

Next, the total aircraft drag as a function of airspeed for the two airfoils is considered. Figure 5 shows the drag buildup for the two cases. As expected, it is seen that the induced drag is dominant at low speeds and is small at the high-speed end. At the high speeds, however, the fuselage parasite drag followed by the wing profile drag are the largest contributions to the overall drag. Although these variations in induced, parasite, and profile drag are by no means new, Fig. 5 does put the drag changes due to airfoils in proper context. Another useful piece of information is the crossover point for the two drag curves. From Fig. 3, it was seen that although airfoil Y has better performance below a C_l of 0.65, it has higher C_d for C_l values from 0.65 to the $C_{l\,\max}$ of approximately 1.6. Because of the nonlinear relationship between C_L and the aircraft flight speed V, however, this C_l range of 0.65–1.6 is squeezed into a small V range from approximately 60 to 90 mph, whereas the C_l range of 0.18–0.65 is magnified to a large V range from 90 to 170 mph. This relationship can be better understood by examining the nonlinear C_L scale presented at the top of Fig. 5. As a consequence of this nonlinear relationship between C_L and V, there is a large velocity range over which better aircraft performance is achieved when airfoil Y is selected for the wing.

The power required for level flight is computed in the next step of the process to understand the effects of airfoil changes. Figure 6 shows the power required for level flight, P_{req}, as a function of the flight speed. Also shown is the full-throttle power-available curve based on the assumed engine and propeller characteristics.

Figure 7 shows the variations of aircraft rate of climb and range with airspeed for the two airfoil choices X and Y. The full-throttle rate of climb is computed from the difference between the $\eta_p P_{\text{av}}$ and the P_{req} curves in Fig. 6. It is seen that airfoil X has a better maximum R/C than airfoil Y because this flight condition occurs at low values of V. The maximum level-flight speed at full throttle is the speed at which the R/C is zero. From the curves in Fig. 7, the increase in level-flight maximum speed is computed to be approximately 2 mph as a result of the longer runs of laminar flow when using airfoil Y instead of airfoil X. This increase in $V_{\max}$ due to the increase in laminar flow is dependent on the specific aircraft characteristics. For example, the increase in $V_{\max}$ will be larger for an aircraft with a greater wing area and smaller fuselage equivalent parasite drag area.

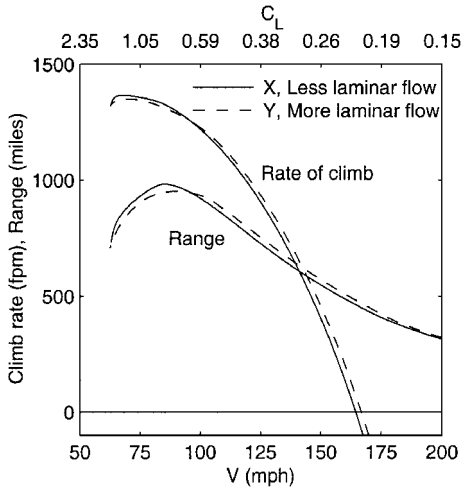

Fig. 7 Variation of aircraft rate of climb and range with airspeed for the airfoil choices X and Y.

Comparison of the range predictions shows that, although airfoil X results in a greater maximum range, the best-range flight speed for airfoil X is less than that for airfoil Y. Most general-aviation aircraft, however, cruise at a speed that is greater than the speed for best range.[14,15] With this consideration, there is a nearly 20-mile (approximately 5% at 125 mph) improvement in range for airfoil Y at all flight speeds from 100 to 165 mph.

The performance-simulation approach described can be a useful tool for putting the effects of changes in airfoil characteristics into proper perspective with the overall aircraft performance. In addition, this approach allows the inclusion of trim effects in computing the aircraft performance. Although this type of performance simulation can be helpful for selecting the best airfoil out of a group of candidate airfoils, it does not give sufficient guidance on how an airfoil should be designed to optimize one or more performance parameters for a given aircraft. Tailoring an airfoil to suit an aircraft with this approach can be a tedious trial-and-error process. To improve the understanding of the airfoil–aircraft connection and to arrive at analytical methods to guide the airfoil design process, the following section presents the second approach that involves derivation of analytical expressions relating airfoil drag polar characteristics to aircraft performance.

Analytical Approach to Airfoil–Aircraft Matching

This section presents the second approach that involves deriving analytical expressions that can be used to tailor an airfoil to suit a particular aircraft. Two performance parameters are considered: level-flight maximum speed and maximum range. For this section, a family of 13 airfoils have been designed, all having 14% maximum thickness-to-chord ratio and the same amount of laminar flow (50%c on the upper and lower surfaces) but with different C_l values for the lower corner of the low-drag range (drag bucket). This family has been designed using PROFOIL[2] and the airfoil inverse design variables discussed in Ref. 6. More specifically, the airfoils in the family were designed by varying the design C_l for the lower surface. As discussed in Ref. 6, this design C_l in turn determines the C_l for the lower corner of the low-drag range, referred to hereafter as C_l^{low}. The resulting airfoil shapes have systematic changes in the camber, although camber was not explicitly specified in the airfoil design.

The 13 airfoils have been labeled A–M, with airfoil A having the smallest C_l^{low} of 0.1, and airfoil M having the largest C_l^{low} of 0.83. In other words, airfoil A has the least camber and airfoil M has the largest camber. Figure 8 shows the geometries and inviscid velocity distributions for 3 of the 13 airfoils, B, H, and L. Figure 9 shows the predicted performance of the airfoils at $Re\sqrt{C_l} = 2 \times 10^6$. It can be seen that the C_d vs C_l variation for each airfoil is linear in the low-drag region and can be described by Eq. (1) for a straight line, referred to as the low-drag line:

$$C_d = C_d^0 + C_l/\beta \tag{1}$$

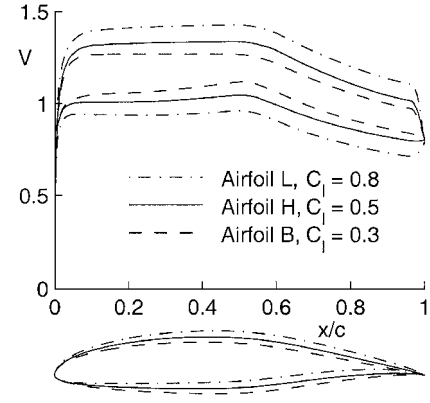

Fig. 8 Inviscid velocity distributions for airfoils B, H, and L.

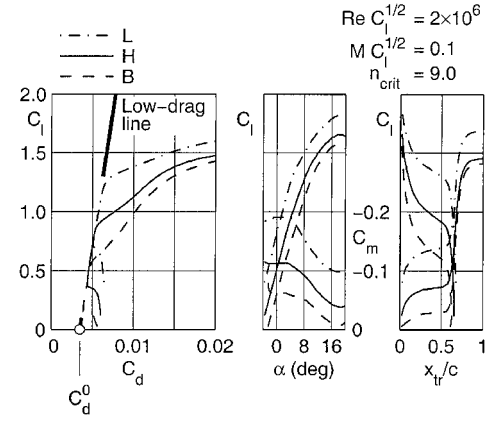

Fig. 9 Performance of airfoils B, H, and L predicted using XFOIL.[3]

where C_d^0 is the C_d intercept of the low-drag line on which the low-drag regions of all of the polars lie and β is the the slope of the low-drag line dC_l/dC_d. In other words, the drag buckets of the different airfoils all lie on the low-drag line described by Eq. (1). With this description, it is possible to look for variations in the aircraft performance parameters as a function of C_l, by fixing the amount of laminar flow for a family of airfoils and, therefore, specifying C_d^0 and β. For the family of airfoils considered in Figs. 8 and 9, the C_d^0 is 0.0035 and β is 467.

In this section, the approach is first adopted to determine the optimum value of C_l^{low} for selecting the most suitable airfoil for an aircraft designed for maximizing the aircraft level-flight maximum speed $V_{\max}$. Then, the variation of range with variation in the operating C_l is studied for points on the airfoil drag polar that lie on the low-drag line: This study provides guidelines for tailoring an airfoil for maximizing the range of an aircraft. The aircraft for these studies is assumed to have the specifications in Table 1. It is realized that the changes in airfoil pitching moment coefficient for the family of airfoils under consideration will result in changes in the drag associated with trimming the aircraft. However, to derive simple expressions to help guide the tailoring of an airfoil to suit an aircraft, the trim effects on drag are ignored. To isolate the effects of the airfoil changes, the results in the following subsections pertain to the tail-off condition and, thus, do not include the effects of the changes in the drag associated with trim. The consequences of ignoring the trim effects are discussed later in the section on the validation of the analytical approach.

Level-Flight Maximum Speed

To tailor an airfoil to suit an aircraft designed to have as high a $V_{\max}$ as possible, it is necessary to select the airfoil based on C_l^{low} and the $C_{d\,\min}$. From Fig. 9, it can be seen that for a family of airfoils with a prescribed amount of laminar flow, $C_{d\,\min}$ is directly related to the choice of C_l^{low} because they both lie on the low-drag line. For

a given laminar-flow extent, therefore, the selection of the airfoil for the V_{max} condition needs to be made by choosing the optimum value of C_l^{low} from among the points that form the low-drag line. Furthermore, because the power required P_{req} equals $\eta_p P_{av}$, it is instructive to examine the variation of the P_{req} for various points on the low-drag line. This variation of P_{req} along the low-drag line is studied to arrive at an analytical approach to choose the value of the C_l^{low} for the V_{max} flight condition.

When it is assumed that the wing profile drag coefficient C_{Dp_w} is equal to the airfoil C_d, the wing drag coefficient can be expressed as

$$C_{Dp_w} = C_d^0 + C_l/\beta \tag{2}$$

For the tail-off case, the aircraft C_L is equal to the wing C_{Lw}, and C_{Lw} is in turn taken as the average value of the airfoil C_l over the entire wing span. As a result, $C_L = C_l$ for the expressions derived in the analytical approach. The aircraft drag coefficient C_D can be obtained from Eq. (2) by adding the fuselage and induced-drag contributions. The expression for this aircraft C_D is presented in Eq. (3) in terms of C_d^0 and β:

$$C_D = C_d^0 + C_L/\beta + C_{Df} S_f/S_w + C_L^2/\pi e\mathrm{AR} \tag{3}$$

The resulting aircraft drag and power required for level flight are

$$D = \frac{1}{2}\rho V^2\left(C_d^0 S_w + C_{Df} S_f\right) + \frac{W}{\beta} + \frac{2W^2}{\pi b^2 e \rho V^2} \tag{4}$$

$$P_{req} = \frac{1}{2}\rho V^3\left(C_d^0 S_w + C_{Df} S_f\right) + \frac{W}{\beta}V + \frac{2W^2}{\pi b^2 e \rho V} \tag{5}$$

Because of the fact that at the V_{max} flight condition $P_{req} = \eta_p P_{av}$, it is possible to solve for the value of V at which the P_{req} in Eq. (5) equals $\eta_p P_{av}$. This value of V will be the V_{max} for an airplane that has a hypothetical airfoil drag polar that is the low-drag line itself. However, because the C_l^{low} for the most suitable airfoil lies on this low-drag line, this value of V is the V_{max} for the airplane using the most suitable airfoil. From this V_{max}, the wing C_{Lw} and, hence, the C_l^{low} can be calculated by equating the lift and the aircraft weight.

The resulting expression is presented in Eq. (6) by setting $P_{req} = \eta_p P_{av}$ and $V = V_{max}$ in Eq. (5):

$$AV_{max}^3 + BV_{max} + C(1/V_{max}) - \eta_p P_{av} = 0 \tag{6}$$

where

$$A = \left(C_d^0 S_w + C_{Df} S_f\right)(\rho/2) \tag{7}$$

$$B = W/\beta \tag{8}$$

$$C = 2W^2/\pi b^2 e \rho \tag{9}$$

This value of V_{max} and the corresponding C_l^{low} represent the most suitable airfoil for the V_{max} flight condition from among the candidates that share the same value of C_d^0 and β. If the extent of laminar flow is varied to generate several such families with different values of C_d^0, then it is possible to get the locus of the C_l^{low}–$C_{d\ min}$ points for these families. This locus defines the optimum placement for the lower corner of the low-drag range for any airfoil from among the families considered.

Figure 10 shows this locus for the optimum placement of C_l^{low} along with the polar for the most suitable airfoil D for the V_{max} flight condition from among the family of airfoils A–M. It can be seen that if an airfoil is chosen with a C_l^{low} that is above this locus (such as airfoil H or L in Fig. 9) then the airplane has potential for increase in V_{max} by selection of a wing airfoil with less camber. On the other hand, if an airfoil is chosen with the C_l^{low} that is lower than this locus line (such as airfoil B in Fig. 9), then the airfoil has too low a camber for the aircraft, and the portion of the low-drag range below the locus line is not utilized except in a dive. The drawback is that the high-C_l performance is compromised and the airplane has an unnecessarily high stall speed.

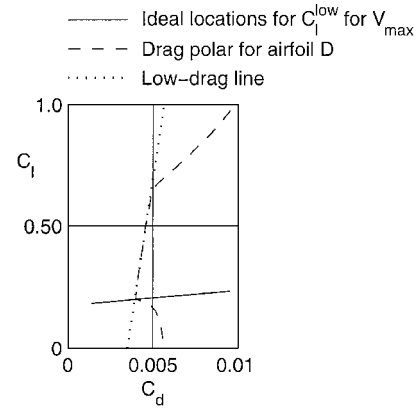

Fig. 10 Ideal locations for C_l^{low} corresponding to level-flight maximum speed along with the drag polar for the most suitable airfoil D and the low-drag line.

Note that these analytical expressions for tailoring an airfoil for the V_{max} condition can also be used to instead tailor the airfoil for the velocity corresponding to level-flight speed at a cruise power setting. In this case, the P_{av} would have to be replaced by the cruise-power setting P_{cruise}. The ideal airfoil for this cruise-power condition would have a C_l^{low} that is higher than the C_l^{low} obtained for the V_{max} condition.

Range

To tailor an airfoil to maximize the range of an aircraft, it is necessary to make the airfoil selection based on the C_l for the upper corner of the low-drag range, or C_l^{up}. Because this upper corner that this upper corner also lies on the low-drag line defined by C_d^0 and β for the family of airfoils with a prescribed amount of laminar flow, it is useful to examine the variation of aircraft range with C_l for points on the low-drag line.

The well-known Bréguet range equation, shown in Eq. (10) for constant values of η_p and specific fuel consumption (SFC) clearly illustrates that range for an aircraft is maximized at the aircraft lift coefficient corresponding to the aircraft maximum (L/D) or minimum C_D/C_L condition:

$$R = \frac{\eta_p}{\mathrm{SFC}}\frac{C_L}{C_D}\int_{W_f}^{W_e}\frac{\mathrm{d}W}{W} \tag{10}$$

Thus, the ideal value of C_l^{up} for an airfoil tailored to maximize the aircraft range can be determined by finding the C_l on the low-drag line that results in minimum aircraft C_D/C_L. From the expression for the aircraft C_D as a function of C_L along the low-drag line in Eq. (3), the expression for C_D/C_L can be determined. With the earlier assumption of $C_L = C_l$, this expression is

$$C_D/C_L = C_d^0/C_l + 1/\beta + C_{Df} S_f/C_l S_w + C_l/\pi e\mathrm{AR} \tag{11}$$

The resulting ideal C_l for maximizing the aircraft range can be obtained by taking the derivative of Eq. (11) with respect to C_l and setting it to zero. The resulting expression for the C_l is

$$C_l = \sqrt{\pi e\mathrm{AR}\left(C_d^0 + C_{Df} S_f/S_w\right)} \tag{12}$$

For the hypothetical aircraft used here, this equation provides a lift coefficient of approximately 0.78. As done earlier, if the value of C_d^0 is varied to generate several families of airfoils with different specifications for the extent of laminar flow, then the locus of points that form the ideal values of the C_l^{up} for each family can be constructed. This locus is shown in Fig. 11 along with the polar for the most suitable airfoil G from among the family of 13 airfoils A–M that have 50%c laminar flow on the upper and lower surfaces and a maximum thickness of 14%c. For the aircraft under consideration, the choice of an airfoil with the C_l^{up} that is below this locus (such as

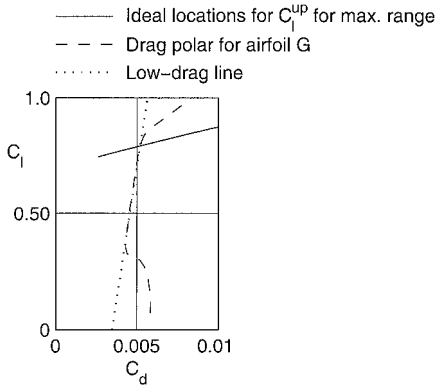

Fig. 11 Ideal locations for C_l^{up} corresponding to maximum range along with the drag polar for the most suitable airfoil G and the low-drag line.

airfoil B in Fig. 9) will mean that the range can be improved by the use of an airfoil with higher camber. On the other hand, selection of an airfoil with the C_l^{up} that is above this locus (such as airfoil L in Fig. 9) will not improve the range beyond that obtained with the use of the most suitable airfoil G, but will only result in a decrease in the low-C_l performance.

Note that the assumption of constant η_p and SFC may not be true in general. This assumption was made to illustrate the analytical approach and to obtain a simple closed-form expression for the ideal C_l^{up}. In a more detailed analysis, it may still be possible to use this approach if the variations in η_p and SFC could be approximated as analytical functions that could then be incorporated in Eqs. (10–12) to obtain a more accurate estimate of the ideal airfoil C_l^{up}.

Trim Considerations

The need to operate an aircraft in a trimmed condition results in three sources of drag[9]: 1) induced drag of the wing–tail system, 2) parasite drag of the tail, and 3) increased wing profile drag due to higher C_{Lw} required with tail download. The performance-simulation approach described in the earlier section for studying the effects of airfoil changes includes all of these three sources of drag. Because of the difficulty in integrating these sources of drag in the analytical expressions, the analytical approach in this section did not consider these sources of drag and were derived for the tail-off condition.

In the following section, the results from the analytical study are compared with the results from the performance-simulation approach, both with and without trim considerations.

Validation

It can be seen from the analytical expressions derived in the preceding section that there are distinct ideal locations to place the upper and lower corners of the low-drag range when tailoring an airfoil for level-flight maximum speed and maximum range, respectively. These ideal locations are compared with the predictions from the performance-simulation approach for the family of airfoils A–M, three of which were previously shown in Fig. 9. These airfoils all have the same amount of laminar flow, but have different locations for the low-drag range.

Figure 12 shows the predicted variations from the performance-simulation approach for V_{max} with change in the airfoil C_l^{low}. The predictions are shown for both the trimmed and the tail-off cases. Figure 12 also shows the ideal value of C_l^{low} of 0.2 from the analytical approach for an airfoil tailored for the V_{max} flight condition. It is seen that as the C_l^{low} is decreased from 0.6 to 0.2 by the use of airfoils with lower camber, there is an increase in V_{max} for both the trimmed and tail-off cases. When the C_l^{low} is decreased below the ideal value of 0.2, however, the further increase in V_{max} is significantly reduced. This distinct slope change in the V_{max} vs C_l^{low} curve validates the analytical expression derived for the V_{max} flight condition and demonstrates that airfoil D is the ideal airfoil for the V_{max} flight condition.

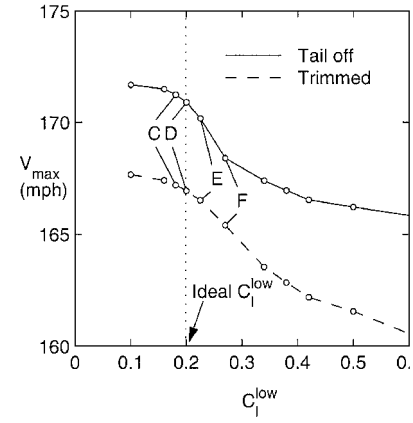

Fig. 12 V_{max} as a function of C_l^{low} for airfoils A–M.

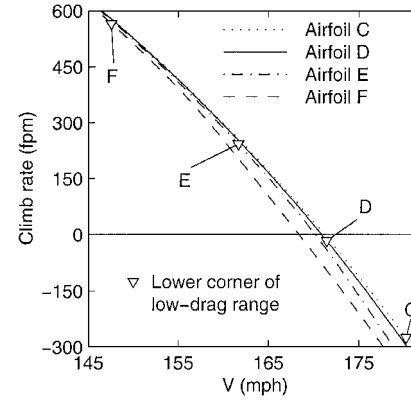

Fig. 13 Rate of climb curves for airfoils C–F illustrating the suitability of airfoil D for the V_{max} condition.

Note that if the low-drag regions for airfoils A–M had lined up perfectly with the assumed low-drag line, then the V_{max} vs C_l^{low} curve for the tail-off case in Fig. 12 would have shown an increase in V_{max} as the C_l^{low} was decreased from 0.6 to the ideal value of 0.2 and an exactly zero increase in V_{max} for any decrease in C_l^{low} below this ideal value. However, the results from the performance-simulation approach do not show the zero increase in V_{max} for $C_l^{low} < 0.2$, but only a distinct reduction in the V_{max} increase. This deviation from the expectations is because of the small deviations in the low-drag regions of the airfoils from the assumed low-drag line. In particular, airfoils A–C have slightly lower C_d than that for the low-drag line for C_l ranging from 0.1 to 0.2.

To more clearly illustrate the effect of the airfoil C_l^{low} on the aircraft V_{max}, Fig. 13 shows the rate-of-climb curves from the performance-simulation approach for airfoils C–F, for which the C_l^{low} values lie in the vicinity of the ideal value of 0.2. These curves have been plotted for the full-power condition. For each of the four airfoils, the point corresponding to the lower corner of the low-drag range is also marked. It is seen that the lower corner for the ideal airfoil D occurs almost exactly at the velocity that results in zero rate of climb, that is, at V_{max}. For airfoils E and F, however, the lower corners are at velocities less than the V_{max} achieved. For this reason, these airfoils have too high a camber. Airfoil C, on the other hand, has the lower corner at a velocity that corresponds to a dive condition. A portion of the low-drag region for this airfoil cannot be used in level flight. Airfoil C, therefore, has too low a camber for the airplane under consideration. Thus, the results in Fig. 13 further demonstrate that airfoil D is the ideal airfoil for the V_{max} condition.

Figure 14 shows the variation in maximum range as a function of C_l^{up}, as predicted by the performance-simulation approach for both the trimmed and the tail-off cases. The predictions for both the cases show that there is a limit for the C_l for the upper corner beyond which there is no improvement in the range. This limit is predicted to be approximately 0.81 for both the cases, and this limit agrees

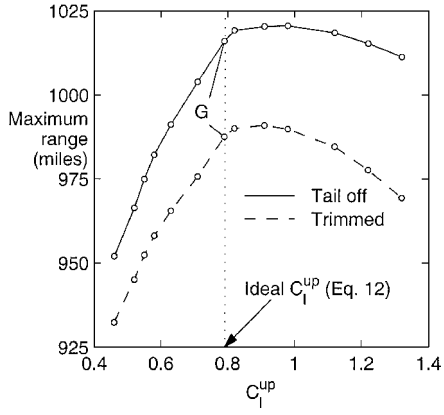

Fig. 14 Maximum range as a function of C_l^{up} for airfoils A–M.

well with the value of 0.78 predicted by the analytical expression in Eq. (12).

Conclusions

With modern inverse airfoil design techniques, it has been possible to design airfoils that have very specific lift, drag, and moment characteristics. However, little guidance was available for tailoring an airfoil to suit a particular application. Toward this objective, two approaches have been presented: 1) an aircraft performance-simulation approach and 2) an analytical approach. In the performance-simulation approach, the changes in airfoil characteristics are used as inputs to an aircraft performance code to predict the resulting changes to the aircraft performance. In the analytical approach, the low-drag portion of the airfoil drag polar is represented by an equation. This equation is used to search for ideal locations of the lower and upper corners of the low-drag range for aircraft designed for level-flight maximum speed and maximum range.

The analytical study shows that there is a distinct ideal value for the lift coefficient of the lower corner of the airfoil low-drag range when the airfoil is tailored for the level-flight maximum speed condition of an aircraft. Likewise, there is a distinct ideal value for the lift coefficient for the upper corner of the airfoil low-drag range when the airfoil is optimized for the maximum range condition of an aircraft. These ideal values for the upper and lower corners of the low-drag range are dependent not only on airfoil parameters, such as the extents of laminar flow on the upper and lower surfaces, but also on the aircraft parameters, such as the drag characteristics of the fuselage and other components, the available power from the engine, and the propeller efficiency. When the performance-simulation approach was used for a family of airfoils with the same amount of laminar flow but with systematic changes in the camber, the analytical expressions for the ideal locations were validated.

The results of the study and the analytical expressions derived provide important criteria for positioning the low-drag range of the airfoil drag polar. In particular, these expressions provide guidelines for tailoring an airfoil to suit an aircraft and can be used to avoid the tedium associated with exploring numerous airfoils in an effort to find the best airfoil for a given aircraft. Although only propeller-driven piston-engine aircraft were considered, the approaches can be extended for use in jet-powered airplanes. Additionally, although the analytical expressions have been developed for airfoils with well-defined low-drag ranges that can be defined by a straight line, the approach can be extended to other types of airfoils (such as low Reynolds number airfoils) by description of the trends in variation of the low-drag range using an appropriate analytical expression. These approaches are likely to be useful to both airfoil and aircraft designers for tailoring an airfoil to suit a particular aircraft. In addition, the expressions developed are suitable for use in an inner loop within an aircraft sizing or multidisciplinary optimization study for selecting the most appropriate airfoil from a family of airfoils.

Acknowledgment

The authors would like to thank Mark Drela for the XFOIL code used in this work.

References

[1]Eppler, R., and Somers, D. M., "A Computer Program for the Design and Analysis of Low-Speed Airfoils," NASA TM 80210, Aug. 1980.

[2]Selig, M. S., and Maughmer, M. D., "Generalized Multipoint Inverse Airfoil Design," *AIAA Journal*, Vol. 30, No. 11, 1992, pp. 2618–2625.

[3]Drela, M., "XFOIL: An Analysis and Design System for Low Reynolds Number Airfoils," *Low Reynolds Number Aerodynamics*, edited by T. J. Mueller, Vol. 54, Lecture Notes in Engineering, Springer-Verlag, New York, 1989, pp. 1–12.

[4]Gopalarathnam, A., and Selig, M. S., "Multipoint Inverse Method for Multielement Airfoil Design," *Journal of Aircraft*, Vol. 35, No. 3, 1998, pp. 398–404.

[5]Drela, M., "Newton Solution of Coupled Viscous/Inviscid Multielement Airfoil Flows," AIAA Paper 90-1470, June 1990.

[6]Gopalarathnam, A., and Selig, M. S., "Low-Speed Natural-Laminar-Flow Airfoils: Case Study in Inverse Airfoil Design," *Journal of Aircraft*, Vol. 38, No. 1, 2001, pp. 57–63.

[7]Selig, M. S., Gopalarathnam, A., Giguère, P., and Lyon, C. A., "Systematic Airfoil Design Studies at Low Reynolds Numbers," *Fixed and Flapping Wing Aerodynamics for Micro Air Vehicle Applications*, edited by T. J. Mueller, Vol. 195, Progress in Astronautics and Aeronautics, AIAA, Reston, VA, 2001, pp. 143–167.

[8]Maughmer, M. D., and Somers, D. M., "Figures of Merit for Airfoil/Aircraft Design Integration," AIAA Paper 88-4416, Sept. 1988.

[9]Kroo, I., "Trim Drag, Tail Sizing, and Soaring Performance," *Technical Soaring*, Vol. 8, No. 4, 1984, pp. 127–137.

[10]Lutze, F. H., "Trimmed Drag Considerations," *Journal of Aircraft*, Vol. 14, No. 6, 1976, pp. 544–546.

[11]Goldstein, S. E., and Combs, C. P., "Trimmed Drag and Maximum Flight Efficiency of Aft Tail and Canard Configurations," AIAA Paper 74-69, Jan. 1974.

[12]Laitone, E. V., "Tail Load Calculations for Light Airplanes," *Journal of Aircraft*, Vol. 31, No. 2, 1993, pp. 466–469.

[13]McKinney, L. W., and Dollyhigh, S. M., "Some Trim Considerations for Maneuvering Aircraft," *Journal of Aircraft*, Vol. 8, No. 8, 1971, pp. 623–629.

[14]Carson, B. H., "Fuel Efficiency of Small Aircraft," AIAA Paper 80-1847, Aug. 1980.

[15]Stinton, D., *The Design of the Aeroplane*, Blackwell Science, Oxford, 1983, pp. 334, 335.